Peer-reviewed version available at Coatings 2018, 8, 472; doi:10.3390/coatings8120472

Article

Optimised performance of non-dispersive infrared gas sensors using multilayer thin film bandpass filters

Pinggui Wang [1,2], Xiuhua Fu [1]*, Des Gibson [2], Lewis Fleming [2], Cheng Li [2], Manu Muhiyudin [2], Shigeng Song [2], David Hutson [2], David Moodie [3], Calum MacGregor [3] and Mathew Steer [4]**

[1] Changchun University of Science and Technology, Changchun 130012, China;
[2] Scottish Universities Physics Alliance (SUPA), The institute for Thin Films, Sensors & Imaging, University of the West of Scotland, Paisley, PA1 2BE, U ;
[3] Gas Sensing Solutions Ltd, 60-62 Grayshill Road Westfield North Courtyard Cumbernauld G68 9HQ, UK;
[4] Scottish Universities Physics Alliance (SUPA), University of Glasgow, ; Glasgow, G12 8QQ, UK;
* Correspondence: 13604435770@126.com; Tel: +86 13604435770
** Correspondence: Des.Gibson@uws.ac.uk; Tel.: +44-(0)771-198-5621

Abstract: In this work performance improvements are described of a low power consumption non-dispersive infrared (NDIR) methane (CH_4) gas sensor using customised optical thin film bandpass filters (BPF). BPF's shape the spectral characteristic of the combined mid infrared III-V based light emitting diode (LED)/ photodiode (PD) light source/ detector optopair, enhancing NDIR CH_4 sensor performance. The BPF, deposited using a novel microwave plasma assisted pulsed DC sputter deposition process, is deposited at room temperature directly onto the temperature sensitive PD heterostructure. BPF's comprise germanium (Ge) and niobium pentoxide (Nb_2O_5) alternating high and low refractive index layers respectively. Two different optical filter designs are progressed; with BPF bandwidths (BWs) of 160 nm and 300 nm. Comparison of modelled and measured NDIR sensor performance is described, highlighting maximized signal to noise ratio (SNR) and minimized cross talk performance benefits. BPF spectral stability for various environmental temperature and humidity conditions is demonstrated.

Keywords: NDIR; methane; sensor; infrared; thin film; III-V, heterostructure; bandpass; microwave; sputter; MBE

1. Introduction

There are increasing requirements to monitor and control the concentration of methane (CH_4) in such fields as environment, landfill sites, fracking facilities, security, industry and agriculture [1-4]. CH_4 is a flammable and explosive gas and is the main component of natural gas. CH_4 becomes explosive when concentration in air are in the range of typically 5% (lower explosion limit (LEL)) [5, 6]. Invisible and odourless CH_4 gas leaks can pose a threat to human life.

Coal mine gas accidents are caused by the rapid increase of methane concentration in a short period of time, not only posing a serious threat to the safety of miners, but can also results in substantial economic losses [5]. In addition to the health and safety of oil & gas industry personnel, CH_4 gas sensing finds relevance in the detection of atmospheric concentrations of CH_4 where increased emissions will contribute to the greenhouse effect. As a result phenomena such as rising temperatures and sea levels and frequent occurrence of extreme weather events will pose a serious threat to food security, ecosystems, and our living environment.

At present, the methods for monitoring methane concentration are based on various detection methods, including electrochemical [7], gas chromatography [8], thermal conductivity [9], catalytic

combustion [10, 11], photoionization [12] and NDIR [13–15]. Among these methods, NDIR gas sensor is the preferred sensing method due to simple operation and maintenance, long service life, fast response time, high measurement accuracy and fail to safe operation [13–15].

NDIR gas sensors comprise an infrared light source, optical BPF and a detector. The light source emits infrared light at a wavelength tuned to the infrared (IR) absorption of gas in the optical path between the source and detector. This results in a reduced IR intensity incident on the photodetector. Typically optical BPF`s are incorporated to improve the NDIR gas selectivity by narrowing the total BW of the spectral response of the source-detector system and thereby preventing cross sensitivity with other gases and water .

By measuring the incident light intensity I_0 and the transmitted light intensity I of the IR light, the concentration of methane gas concentration can be calculated according to the Beer-Lambert law [27]. A state-of-the-art NDIR CH_4 gas sensor has been utilised for this work [16], utilizing a molecular beam epitaxy grown pentanary alloy light emitting diode (LED) light source and photodiode (PD) detector, shown in figure 1(a). For this work the stoichiometry of the semiconductor source-detector pair is tuned for maximum spectral response at 3.3 μm, coinciding with a principle absorption band of the CH_4 molecule, due to the asymmetric stretch vibrational mode [20].

This work describes direct deposition of BPF`s directly onto the LED/ PD optopair, thereby optimizing spectral response shape. A room temperature deposition method suited to direct deposition onto the temperature sensitive LED/ PD optopair is described and associated optical BPF environmental (temperature and humidity) performance.

2. Relevant Background Work & Non Dispersive Infrared Sensor Configuration

Work was previously carried out by Fleming et al [17] in the deposition of 300 nm BW bandpass filters onto commercially available LEDs and photodiodes. This previous work related to carbon dioxide (CO_2) detection for breath monitoring (capnography) during surgical anaesthesia [18, 19]. It was found that application of the coating onto the photodiode only (as opposed to coating the LED only or both LED and PD) with the bandpass filter design was the optimum method to isolate the CO_2 absorption band and reduce cross-talk effect from the commonly used surgical anaesthetic gas nitrous oxide (N_2O) [28]. The light emitted from the mid infrared LED is reflected from a gold coated injection moulded plastic dome geometry optic onto the PD. A CH_4 mid infrared absorption band at 3.3 μm coincides with a CH_4 anti-symmetric stretch vibrational mode. Another band exists in the long-wave infrared (LWIR) and peaks at 7.6 μm. According to HITRAN database [20], the absorption intensity of methane gas is the largest at wavelength 3.3 μm and as such this band was chosen for CH_4 detection in this work.

(**a**) (**b**)

Figure 1. Schematic of the CH_4 gas sensor (**a**) without and (**b**) with optical filter

For this reason, a bandpass BW of 300 nm is chosen for this work, and builds upon the previous work by comparing the effect of a narrower BW (160 nm) bandpass filter. A BW of 300 nm was originally chosen as this matches the BW of the 3.3 μm CH_4 absorption band. The optical coating designs were built into a comprehensive NDIR gas sensor Mathcad model and their effects on the sensor signal accuracy and reduced cross sensitivity determined, specifically adjacent water absorption band at 2.8 μm [20]. A gas sensor model predicting the measured sensor signal as a function of gas concentration was established using Mathcad [21]. The model includes the temperature dependent LED spectral emission and PD spectral detectivity using a generalised form of the Planck equation [22, 23]. Gas species' spectral absorption characteristics are imported from the HITRAN database and are used to model the effect on the sensor signal as a function of gas concentration, comprising various gas mixtures in the sensor light source/ detector optical path length using the Beer-Lambert law. The model includes influence of Johnson-Nyquist noise, dark noise and also quantisation noise is a result of the modelled data collection electronics. Theoretical description of the model is provided in Section 3 of this paper.

Figure 2 shows the modelled and measured spectral response of the CH_4 sensor indicating good agreement between the theoretical and experimental result. Also plotted in figure 2 are the absorption coefficients for CH_4 and water vapour (H_2O). It can be seen that the CH_4 absorption band peak coincides with the peak of the sensor spectral response for both the modelled and experimental curves. The H_2O absorption peak lies in close proximity to the CH_4 peak and as a result, lies within the spectral response of the CH_4 sensor, suggesting that the sensor will suffer from cross-talk (i.e. unwanted signal contribution) from H_2O if it is present in any significant concentration. When the sensor chamber contains water vapour, this can cause significant inaccuracies in detected CH_4 concentration. Therefore, it is advantageous to use optical filtering to reduce the influence of other gases and improve the selectivity of the detection system. In addition, different bandpass filter designs can provide a method to influence the NDIR gas sensor detection accuracy and sensitivity. The primary purpose of this paper is to design the technical parameters of the bandpass filter according to the demand of the NDIR gas sensor and demonstrate room temperature direct deposition onto the LED/ PD optopair, removing the need for inclusion of a separate discrete bandpass filter.

Preprints (www.preprints.org) | NOT PEER-REVIEWED | Posted: 7 October 2018 doi:10.20944/preprints201810.0120.v1

Peer-reviewed version available at Coatings 2018, 8, 472; doi:10.3390/coatings8120472

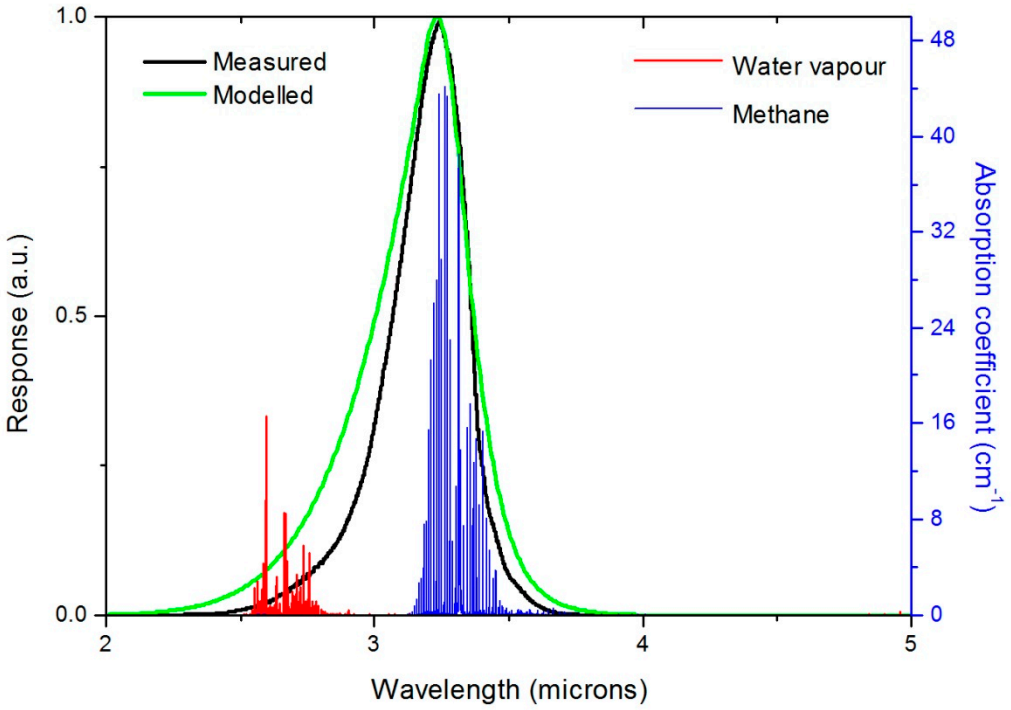

Figure 2. Modelled total sensor spectral response, semi-empirical sensor response and CH_4 and H_2O absorption coefficients.

3. Theoretical Background

3.1. Determination of bandpass filter parameters

The total gas sensor spectral response is determined by

$$G(\lambda) = S(\lambda) * D(\lambda), \quad (1)$$

where S is the spectral response of the source and D is the spectral response of the detector. The gas sensor will be sensitive to any gas with an absorption band that lies within the spectral region of G. When a gas species is present with an absorption band that lies within G, the spectral response follows:

$$G(\lambda) = S(\lambda) * T_g(\lambda) * D(\lambda), \quad (2)$$

where Tg is the optical transmittance of the gas which follows the well-known Beer-Lambert law:

$$T_g(\lambda) = exp(-\alpha(\lambda) * c * l), \quad (3)$$

Where; α is the absorption coefficient of the gas, c is the concentration and l is the pathlength that the light travels through. Analogously, the total spectral response of the source-detector system can be modified by using an optical interference filter with optical transmittance T_f. The new total spectral response for a filtered sensor G_f becomes:

$$G_f(\lambda) = S(\lambda) * T_f(\lambda) * D(\lambda), \quad (4)$$

To maintain maximised NDIR sensor sensitivity to the target gas, the T_f must have maximum optical transmittance over the gas absorbing spectral region and necessary blocking of unwanted signal contributions from other gases and water vapour. T_f must be as close to zero as possible over the absorbing regions of such gases. In this work an optical bandpass filter spectral characteristic mathematical function was modelled using Mathcad 15 and incorporated into a comprehensive gas sensor model. The LED source emission was approximated using the generalised Planck equation and the photodiode detectivity was modelled using the characteristic equations for a photodiode response [24]. From this the modelled NDIR gas sensor signal response incorporating bandpass filter was modelled. The multilayer bandpass filter structure was modelled using thin film optical design software TFCalc, where the multilayer optical filter structure was designed such that the modelled optical transmittance matched that of the bandpass filter spectral characteristic function modelled in the Mathcad NDIR gas sensor program. From the TFCalc [29] model, the exact layer thicknesses and number of layers for each coating design were used as the basis for experimental deposition of the multilayer bandpass filters. The influence of 2.67 μm infrared absorption peak of water vapour, angle offset and signal-to-noise ratio were taken into account during the filter design stage. Two different bandpass filters (table 1) were designed based on sensor signal modelling results (table 2) for maintaining good sensor accuracy up to the CH_4 LEL and good blocking of H_2O absorbing wavelengths that are a considerable cause of cross-talk for this sensor design. The results show that the accuracy of 300 nm is lower than the accuracy of 160 nm, but is still highly adequate.

Table 1. Comparison of technical parameters between 160 nm and 300 nm band pass filter

Bandpass Filter Parameter	160 nm BW filter	300 nm BW filter
Central wavelength (μm)	3.3	3.325
FWHM (nm)	160	300
T (peak)	73%	85%
Blocking (μm)	2-5	2-5

Table 2. Comparison of accuracy between 160 nm and 300 nm band pass filter

CH_4 concentration range (ppm)	160 nm BW filter (%)	300 nm BW filter (%)
10 – 100	6.2	7.7
100 – 1000	0.6	0.8
1000 – 50000	0.01	0.02

3.2. Design of the 300 nm and 160 nm BW optical bandpass filters

A three cavity Fabry-Perot BP was modelled in TFCalc, as a starting design for both the 300 nm and 160 nm BW bandpass filters. Next, a computational optimisation technique was used to alter the multilayer design in order to achieve two different bandpass filter designs, one with a 300 nm and one with a 160 nm BW passband, both with good out of band blocking to reduce signal contributions from other gases.

For the 300 nm BW bandpass filter, the structure consists of 34 layers and the total thickness is 10.6 um, the peak transmittance reached 60%, while the average transmittance in the out of band regions, 2-3 μm and 3.6-5 μm are 0.09% and 0.32%, respectively, and the SNR of filter is 2.4%. For the bandpass filter with BW of 160 nm, the number of layers was 30 with a total thickness of 9.6 um, the

Preprints (www.preprints.org) | NOT PEER-REVIEWED | Posted: 7 October 2018 doi:10.20944/preprints201810.0120.v1

Peer-reviewed version available at Coatings 2018, 8, 472; doi:10.3390/coatings8120472

peak transmittance reaches 58%, the average blocking area of 2-3.1 μm and 3.5-5 μm is 0.12% and 0.31%, with a SNR of 4.5%.

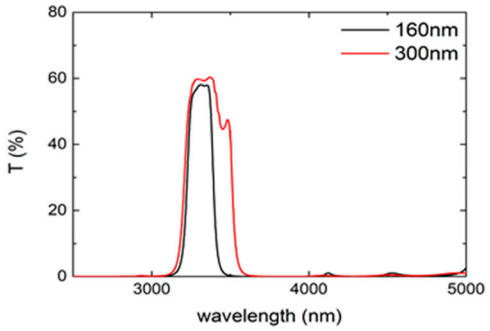

Figure 3. Measured spectral characteristics for optimised 300 nm BW bandpass and 160 nm BW bandpass filter designs.

4. BPF Deposition Method & Materials

4.1. Multilayer thin film optical interference filter preparation method

In this work, thin film optical coatings were prepared using a novel microwave plasma-assisted pulsed reactive DC magnetron technique. The system used is shown in figure 4. The apparatus is equipped with a complete microwave generator system comprising a 6 kW microwave magnetron head, tuner and microwave delivery tubes. Reactive plasma ion density is greatly enhanced via use of this external microwave source, which results in a greater reactive gas reactivity and generates a greater number of monoatomic ions which results in greater coating uniformity and reduced optical absorption in the applied coatings. Use of pulsed DC power greatly reduces the problem of arcing caused by target poisoning and positive charge build up on the sputtering target surface and aids achieving a higher film deposition rate. In this work, thin films Ge and Nb_2O_5 were obtained by sputtering from Ge and niobium (Nb) bulk sputtering targets, each with 99.999% (5N) purity.

The deposition rate and thickness of the film are monitored in real-time by quartz crystal thin film thickness monitors [30], utilsing three crystals per magnetron. Argon is used as sputter process gas and oxygen as a reactive gas. At the same time, the pressure and flow rate of gas are accurately controlled by an optical gas controller (OGC) and MKS mass flow controllers controlled by a multi-gas controller. The chamber body is heated by hot water to liberate any residual H_2O molecules trapped on the chamber walls and into the molecular flow regime, thereby increasing their probability of becoming trapped by Meisner cooling coils in the vacuum chamber (Telemark polycold model 3600).

Removal of water vapour is essential for the growth of high quality mid-infrared optical coatings where film density and water content play a significant role in determining the films optical absorption and spectral stability. Typical system ultimate vacuum is 5×10^{-7} mbar, minimizing adverse influence of water vapour on the optical BPF performance of the film is reduced. By adjusting deposition process parameters, required quality and low absorption Ge and Nb_2O_5 single layer films were deposited for optical characterization, essential for the design and manufacture of multilayer thin film optical BPF`s. Specific process parameters used are shown in Table 3. This system was used to deposit two different BPF`s - specifically 300 nm BW and 160 nm BW, directly deposited onto Gas Sensing Solutions (GSS) Ltd NDIR gas sensor photodiodes for comparison of influence on gas sensor performance. Also included in each coating run was a 100 mm (4") undoped <100> Czochralski grown silicon (Si) wafer, and gallium arsenide (GaAs) witness pieces.

Preprints (www.preprints.org) | NOT PEER-REVIEWED | Posted: 7 October 2018 doi:10.20944/preprints201810.0120.v1

Peer-reviewed version available at Coatings 2018, 8, 472; doi:10.3390/coatings8120472

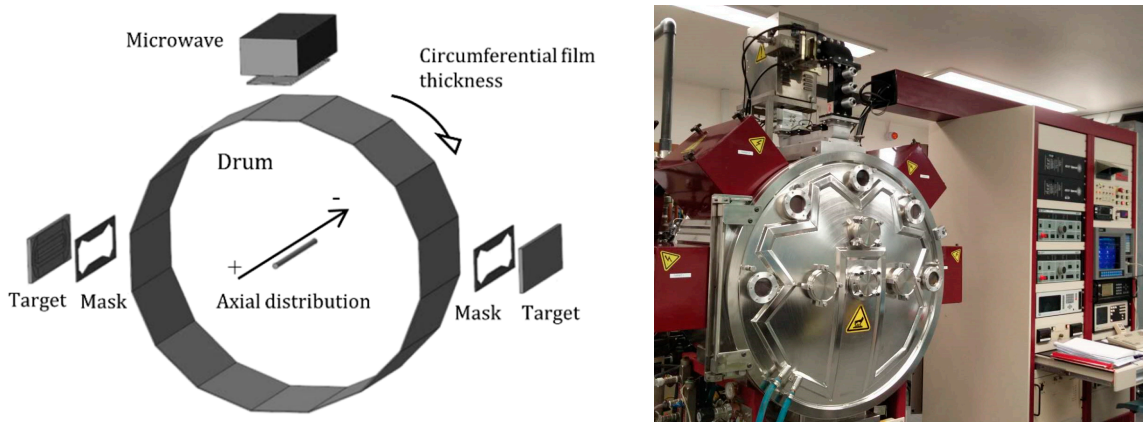

Figure 4. (a) Schematic of the microwave plasma-assisted sputter reactor used to deposit thin optical films described in this work and (b) image of the actual chamber. Right and left hand side magnetrons were used, populated with Ge and one Nb target material.

Table 3. Deposition process parameters used to grow thin films of Ge and Nb_2O_5. 10 kW Advanced Energy magnetron drive (MDX) power supplies were used in voltage regulation and current regulation mode for Ge and Nb_2O_5 respectively to drive the sputtering process.

Material	Ge	Nb_2O_5
MDX power (kW)	2.5	2.84
MDX current (A)	6.1	7.75
MDX voltage (V)	410	367
Argon flow ($sccm^{-1}$)	190	190
O2 flow ($sccm^{-1}$)	0	75
O2 partial pressure (Torr)	0	$6*10^{-4}$
Microwave plasma power	0	3
Deposition rate (nms^{-1})	0.1	0.18

4.2. Optical characterization

Optical transmittance in the mid-IR for single and multilayer coatings were obtained using a Nicolet iS-50 Fourier Transform Infrared (FTIR) spectrometer. The optical constants which are essential for multilayer thin film optical filter design (refractive index and absorption coefficient) were derived from the optical transmittance spectra using a combination of the O'Leary, Johnson and Lim (OJL) model [25] for amorphous materials and the Drude model. The TFCalc thin film design software was then used to design a band pass filter meeting the required specification, and calculate the deviation between the design and the experimental results. Gas sensor photodiode spectral photocurrent response for uncoated and coated diodes was measured using a Bruker VERTEX 80/80v FTIR, configured such that the IR beam was incident on the photodiode under test.

4.3. Gas sensor testing

Calibrated gas sensors were placed in a testing chamber at room temperature and exposed to a gas mixture of N_2 (which is IR inactive so does not elicit a response in the sensor) and CH_4. The CH_4 concentration was controlled by varying the continuous flow rate ratio provided by a CH_4 mass flow controller (MFC) and an N_2 MFC. A range of 0 ppm – 50000 ppm CH_4 was used and was chosen as 50000 ppm is the LEL for CH_4.

5. Results & Discussion

5.1. Thin film optical constant derivation

Single layers were deposited onto 500 µm thick gallium arsenide (GaAs) substrate. Optical transmittance spectra for single layer 1 µm Ge and 1.5 µm Nb_2O_5 as measured using FTIR is shown in figure 5 and overlain with the uncoated GaAs substrate spectrum for comparison. The calculated optical constants are shown in figure 6. It can be seen that the absorption coefficient of the thin film materials are small, and the refractive index contrast between the Ge and Nb_2O_5 thin films is large, suggesting that these materials are acceptable material candidates for use in the fabrication of mid infrared multilayer optical BPF`s.

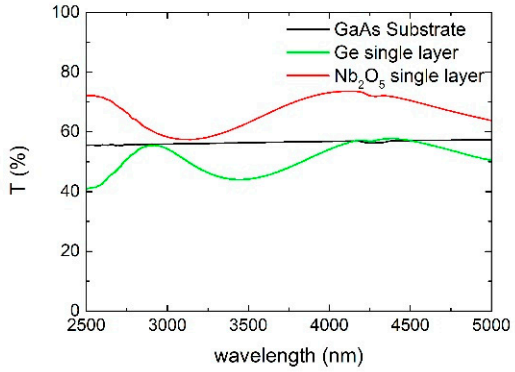

Figure 5. Optical transmittance spectra of GaAs substrate, Ge single layer and Nb_2O_5 single layer.

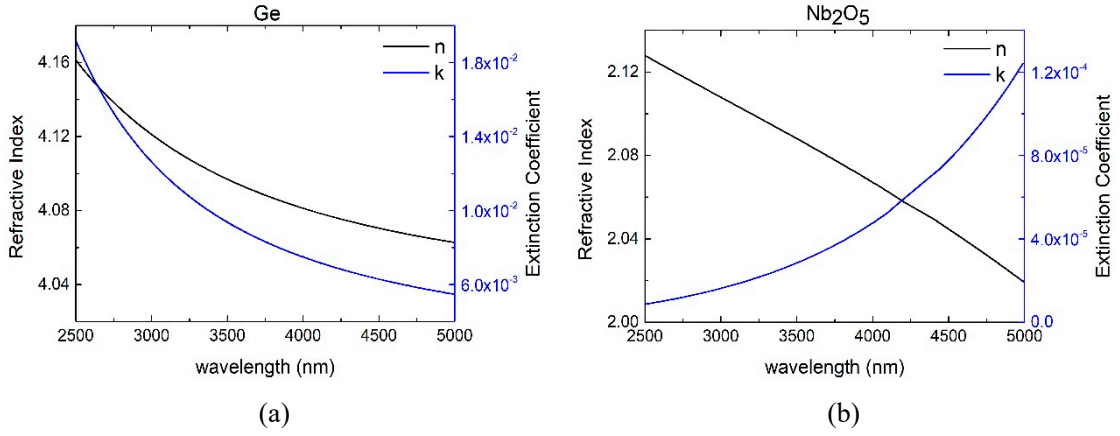

(a) (b)

Figure 6. Optical constants for (a) thin film Ge and (b) thin film Nb_2O_5 as calculated by using a combination of the OJL and Drude models.

5.2. Multilayer thin film optical interference bandpass filter deposition

Two different bandpass filter Ge/Nb_2O_5 multilayer designs were deposited onto GSS methane sensor photodiodes using precision laser cut masking to mask the rest of the bridgeboard LED structure. The spectral transmittance characteristic curve of each bandpass filter was obtained using the Nicolet iS-50 FTIR on the witness samples present during the coating runs. Figure 7 shows excellent agreement between the theoretical design and measured results of the two optical BPF`s. It can be seen that the actual transmittance of the 160 and 300nm BPF`s are 57% and 58% respectively, in excellent agreement with the design values. This is because deposited thickness was greater than the model resulting in a slightly higher optical absorption. However, this slight mismatch between theory and design is negligible as the bandpass CWL and BW remains the same – the two critical parameters for maintaining gas sensor sensitivity to CH_4 and for out of band blocking of the H_2O infrared absorption band centred at 2.67 um. Bandpass filter design parameters for 160 nm BW and 300 nm BW are shown in table 1.

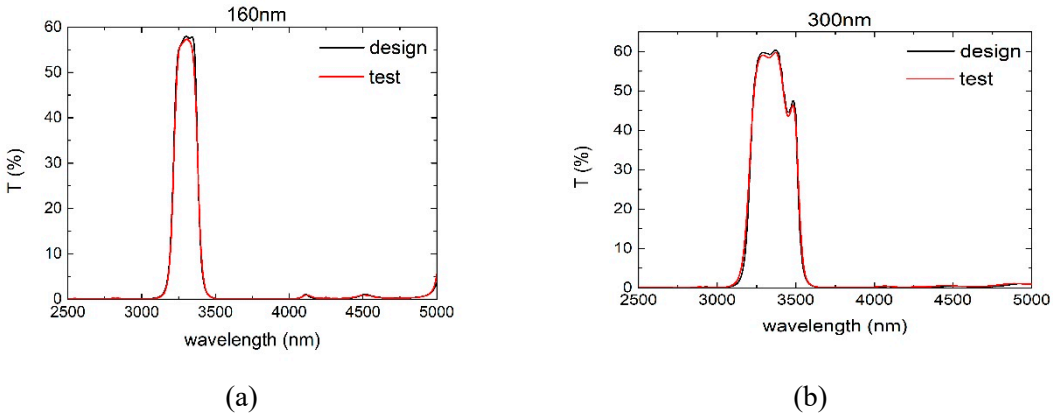

(a) (b)

Figure 7. Comparison between theory and experimet for (a) 160 nm BW bandpass filter and (b) 300 nm BW bandpass filter designs.

5.3. Uncoated and coated gas sensor photodiode photocurrent spectral response

The aforementioned coatings were applied to the GSS CH_4 gas sensor LED/ PD bridgeboards tuned for emission and detection at the CH_4 absorbion wavelength at 3.3 μm. The bridgeboard was masked apart from the photodiodes, enabling the optical coating to be applied to the photodiode. Using a Bruker VERTEX 80/80v FTIR, the spectral response for the uncoated and coated diode heterostructure was recorded. Figure 8 shows the BPF influence on the photodiode photocurrent response when illuminated with broadband IR radiation.

Preprints (www.preprints.org) | NOT PEER-REVIEWED | Posted: 7 October 2018 doi:10.20944/preprints201810.0120.v1

Peer-reviewed version available at Coatings 2018, 8, 472; doi:10.3390/coatings8120472

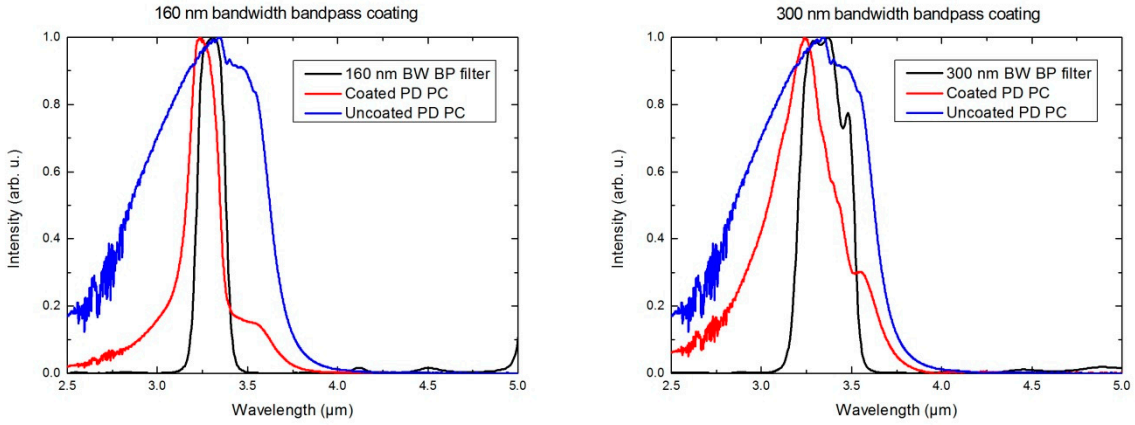

(a) (b)

Figure 8. Overlay of coated and uncoated CH_4 photodiode photocurrent response coated with (a) 160 nm BW bandpass filter and (b) 300 nm BW bandpass filter. The spectral characteristics for the measured witness samples are also shown. It can be seen that in both cases, the photodiode photocurrent response shapes conform to the shape of the optical filter spectral characteristic.

It can be seen that the coated photodiode photocurrent response is shaped by the optical filter spectral transmittance characteristic. Application of the optical BPF provides significant reduction in photodiode BW photocurrent response, and hence the total sensor spectral response is reduced, lowering the response at wavelengths outwith the CH_4 absorption band with the aim of minimising sensor response to gases other than CH_4 and also improving the accuracy of the sensor for the CH_4 target gas. Here it is demonstrated that different optical filter designs can be readily applied to the sensor photodiode, allowing for a greater flexibility in sensor design and the ability to customise and optimise NDIR gas sensor design to specific customer applications.

5.4. Gas sensor testing results

The signal as a function of time for a 160 nm BW BP and a 300 nm BW BP coated sensor is shown in figure 9. The sensors were calibrated for temperature compensation and then exposed to a nitrogen (N_2)/CH_4 gas mixture where the CH_4 concentration was cycled between 0%, 2.5% and 5% CH_4 concentration over a duration of 4 hours. From figure 9, it can be seen that both the 160 nm and 300 nm BW BP coated sensors show a similar response to this variation in CH_4 concentration. As expected, the SNR performance of the 300 nm BW BP coated sensor is superior to the 160 nm BW BP sensor as a result of a greater intensity of IR light transmitted through the BPF.

Preprints (www.preprints.org) | NOT PEER-REVIEWED | Posted: 7 October 2018 doi:10.20944/preprints201810.0120.v1

Peer-reviewed version available at Coatings 2018, 8, 472; doi:10.3390/coatings8120472

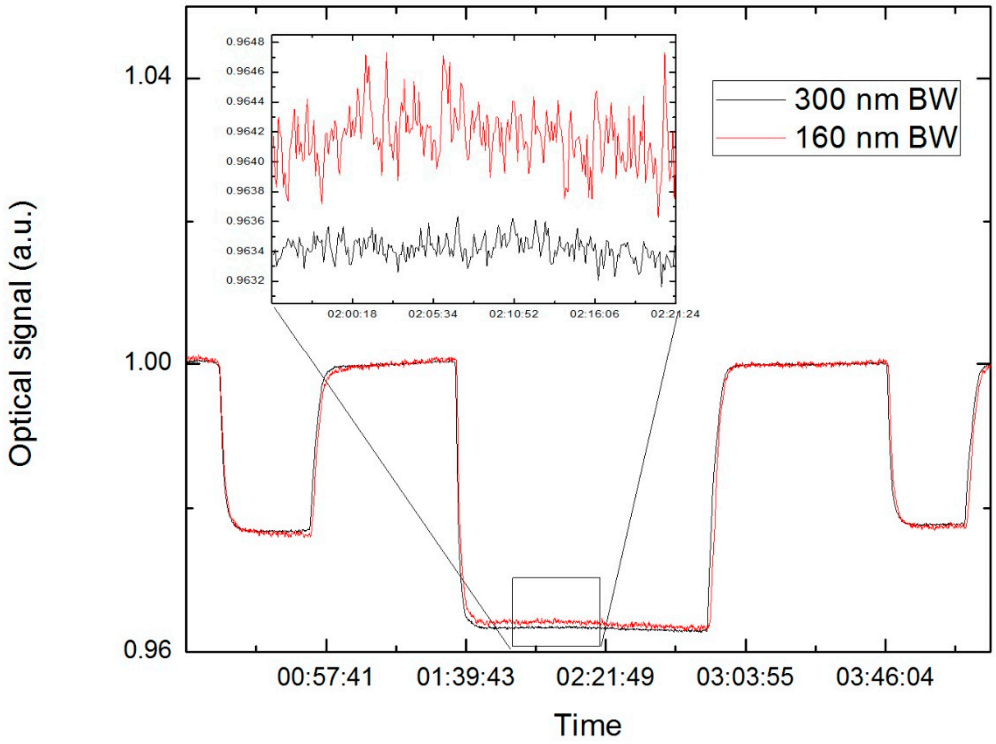

Figure 9. Calibrated sensor signal response for 160 nm BW BP and 300 nm BW BP coated sensors when cycled from 0 ppm, 25000 and 50000 ppm methane (LEL) over the course of 4 hours. Inset plot shows an exploded view of the signal at 5% methane, highlighting the different noise characteristic between the 300 nm BW BP coated sensor and the 160 nm BW BP coated sensor.

For this reason, we suggest it is suggested the 300 nm BW BP filter is a better choice than the 160 nm BW BP filter as it has an improved SNR performance. Table 4 shows the calculated root-mean-square (RMS) noise for 5%, 2.5% and 0% CH_4 for both the 160 nm BW BP coated and 300 nm BW BP coated sensors. Generally RMS noise increases with increasing gas concentration as more light is absorbed and less light is incident on the sensor photodiode. The calculated values for 2.5% and 0% methane for the 160 nm BW BP sensor do not reflect this, however the authors suspect this to be due to the small sample size collected for 2.5% methane.

Table 4. Calculated RMS noise for 160 nm and 300 nm BW BP coated sensor signals.

Methane percentage (%)	160 nm BW BP coated sensor (a.u.)	300 nm BW BP coated sensor (a.u.)
5	3.6×10^{-4}	1.9×10^{-4}
2.5	2×10^{-4}	1.8×10^{-4}
0	2.4×10^{-4}	1.1×10^{-4}

5.5. Wafer uniformity test

Work has previously been carried out by Cheng et al [26] in testing coating thickness uniformity in the using the microwave plasma-assisted sputtering technique used in this work. In this work, the

Preprints (www.preprints.org) | NOT PEER-REVIEWED | Posted: 7 October 2018 doi:10.20944/preprints201810.0120.v1

Peer-reviewed version available at Coatings 2018, 8, 472; doi:10.3390/coatings8120472

bridgeboards were mounted onto specially designed tooling with precision masking in order to apply the coating to the photodiode surface area only, however, this method may not be optimal for scalable mass production of coated photodiodes. A more optimal method would be to sputter deposit the coating onto an enitre photodiode wafer directly after it has been grown by MBE prior to dicing and mounting onto sensor bridgeboards. For this reason, both the 160 nm and the 300 nm BW bandpass filter optical coating designs were each successfully deposited onto 100 mm diameter (4") <100> undoped silicon (Si) wafers with 500 μm thickness grown by the czochralski method and tested for coating uniformity to demonstrate that the bandpass filter spectral characteristic is uniform over an entire 4" wafer and thus suitable for coating an entire newly grown photodiode wafer.

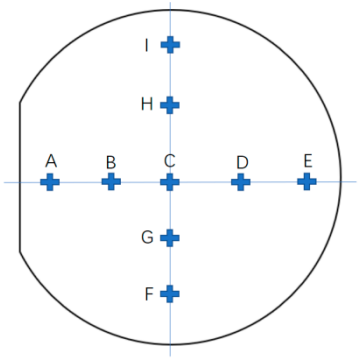

Figure 10. Schematic of 4" Si wafer as mounted onto the microwave plasma-assisted sputter coater drum. Post-coating, the wafer was diced into 20 x 20 mm sections and the optical transmittances was measured for samples A – I to test for coating thickness uniformity. This was done for both 300 nm and 160 nm BW bandpass filters.

The Si wafer was mounted onto the deposition system's rotating drum such that the wafer flat was parallel with the circumference of the drum as depicted in figure 10. Post coating, the wafer was then diced into 20 x 20 mm squares and each section's position was labelled and measured using FTIR to compare the spectral variation in their optical transmittances. The results for the 160 nm and 300 nm BW bandpass filters are plotted in figure 11.

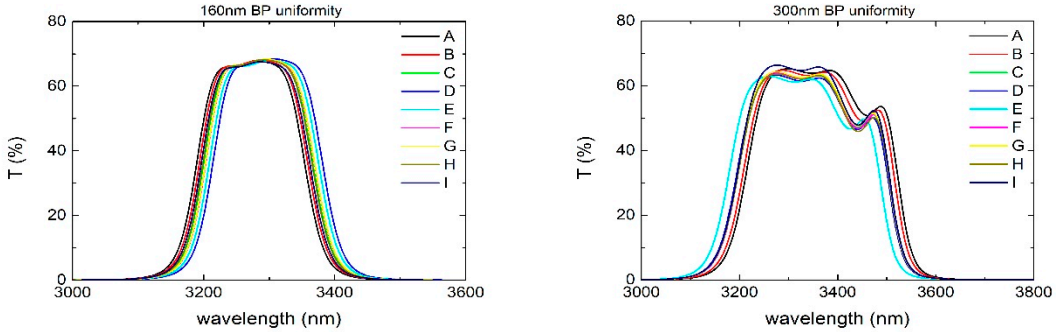

(**a**) (**b**)

Figure 11. (**a**) Optical transmittance spectral characteristics for different Si wafer location samples A-I for the 160 nm BW bandpass filter. (**b**) Optical transmittance spectral characteristics for different Si wafer location samples A-I for the 300 nm BW bandpass filter.

Preprints (www.preprints.org) | NOT PEER-REVIEWED | Posted: 7 October 2018 doi:10.20944/preprints201810.0120.v1

Peer-reviewed version available at Coatings 2018, 8, 472; doi:10.3390/coatings8120472

From these spectra, the coating uniformity was calcaulted for both the 300 nm badwidth bandpass filter and the 160 nm BW bandpass filter and the results are shown in table 4.

Table 4. Thickness uniformity across a 4″ Si wafer for two different optical filter designs.

Filter BW (nm)	Thickness uniformity from center of the 4″ Si wafer (%)
160	±0.355
300	±0.530

These small deviations show that satisfactory coating thickness uniformity can be achieved across an entire wafer maintaining the desired optical transmittance spectral characteristic by maintaing good optical transmittance over the CH_4 absorption band and adequate blocking at H_2O absorption wavelengths, suggesting that coating an entire photodiode wafer prior to dicing and mounting onto electronics bridgeboards may be a production efficient way of incorporating optical filters into NDIR gas sensor architectures.

5.6. Accelerated lifetime testing

A common accelerated lifetime test to probe the optical and structural integrity of thin film coatings is to use subject the samples to the pressure cooker test, where coated witness samples are subjected to a prolonged exposure to high temperature and high pressure using a pressure cooker. Perhaps more relevant to optics in extreme conditions such as those for high velocity windows for military aircraft or coatings for machinery tooling, the pressure cooker test is a good indicator of coating durability in harsh environments. The center piece of the coated Si wafer for both the 160 nm BW bandpass and the 300 nm BW bandpass were placed into the cenetr of a pressure cooker with maxiumum pressure of 15 psi. The samples were subjected to cooking times of 5, 10, 20 and 40 minutes and had their optical transmittances measured by FTIR in between each step.

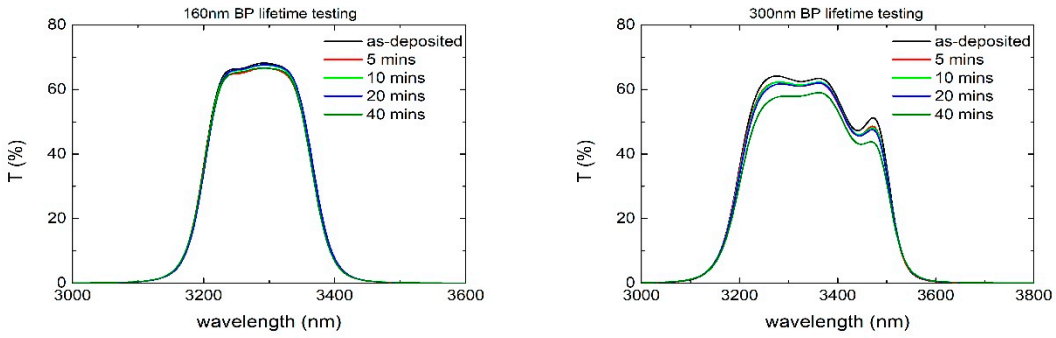

(a) (b)

Figure 12. Optical transmittance of (a) 160 nm and (b) 300 nm BW bandpass witness sample after being subjected to 15 psi inside a pressure cooker for varying durations.

From figure 12 it can be seen that the optical filter spectral characteristic remained largely the same for all times, where a small reduction in peak transmittance was observed for the 160 nm BW bandpass filter. For the 300 nm BW bandpass filter the only minimal change in peak optical transmittance occurred for 5, 10 and 20 minutes, however, the drop in transmittance was more pronounced for 40 minutes. For Differences between the 160 nm BW and the 300 nm BW bandpass samples are most likely to be attributable to the top layer being different, where for 160 nm, the top layer was Ge and for 300 nm it was Nb_2O_5.

The diode surface that the coatings were applied to is an unpolished underside of GaAs (so-called flip-chip method was used to bond the sensor diodes to the electronic bridgeboard, where the upwards facing surface of the element is the backside of the substrate that the MBE grown material was deposited on) therefore factors such as high substrate surface roughness may also be a factor in determining the coatings mechanical integrity for the actual gas application sensing, however, coatings applied to the gas sensor photodiode element will not be subjested to such a harsh environment, so it can be safely assumed that disruption of the coatings optical properties is unlikely to occur.

5.7. Humidity & temperature testing

Gas sensors in different temperature and humidity environment, the performance parameters will be changed, so it is necessary to do the humidity and temperature tests of the optical filter. The closed central pieces of the coated Si wafer for both the 160 nm BW bandpass and the 300 nm BW bandpass were placed into the WKL Temperature and Climatic Test System. The humidity test was carried out at 50 ℃ and 95% humidity for 24 hours and the temperature test is -40 ℃ to 70 ℃ where the temperature was increased by 10 ℃ every two hours.

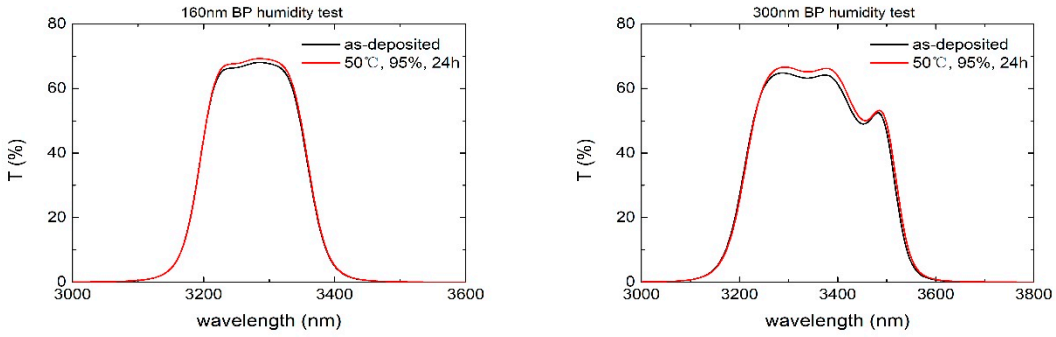

(a) (b)

Figure 13. Optical transmittance of (a) 160 nm and (b) 300 nm BW bandpass witness sample after humidity test.

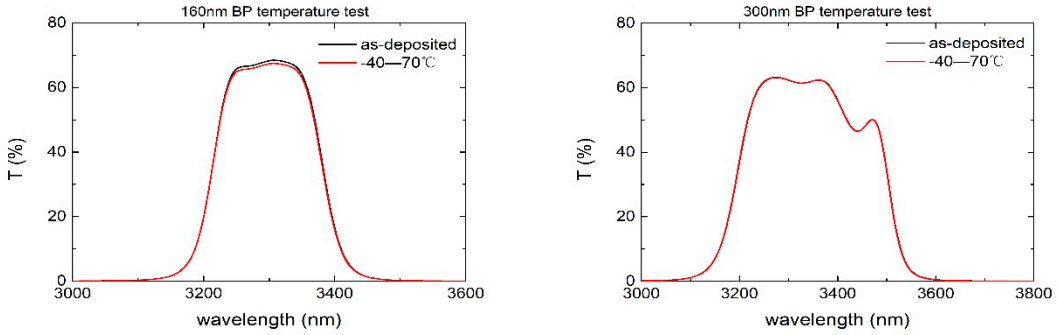

(a) (b)

Figure 14. Optical transmittance of (a) 160 nm and (b) 300 nm BW bandpass witness sample after temperature test.

6. Conclusion

In this work, the spectral response of a methane sensor comprising a heterostructure LED and PD optopair was modelled and compared with the experimentally measured spectral response giving good agreement. The accuracy of such an NDIR gas sensor was modelled from the modelled spectral response. Next, single layers of Nb_2O_5 and Ge were deposited onto optical substrates and optically characterized to obtain their refractive indices and extinction coefficients which were subsequently used in the design of two multilayer optical interference BP filters; one with a passband of 300 nm BW and one with 160 nm BW. These designs were then sputter deposited onto MBE grown heterostructure diodes with peak detectivity tuned to 3300 nm (in order to coincide with the CH_4 absorption band to be used in the interest of CH_4 gas detection) using microwave plasma-assisted pulsed DC magnetron sputtering. The thin film multilayer filters were also deposited onto full 4" Si wafers in the same coating run. The coated and uncoated PD PC responses were measured using a FTIR and it was demonstrated that the PD PC spectral response conforms to the spectral shape of the applied optical filter for both 300 nm and 160 nm BW BP filters. These coated PDs were then built into gas sensor electronics with full injection molded plastic optics and tested under various CH_4 gas concentrations for comparison. Gas concentration was cycled from 0%, 2.5% and 5% CH_4 concentration, to test the sensor's capability in measuring concentrations of CH_4 below the LEL. As expected it was observed that the 160 nm BW BP coated sensor displayed more noise as compared with the 300 nm BW BP sensor, most likely due to the reduced intensity of IR incident of the PD and therefore a poorer SNR. The 160 nm BW BP coated sensor, having a narrower BW as compared with the 300 nm BW BP coated sensor, will be less susceptible to cross-talk inducing gases, so it is difficult to assess which optical coating design is superior given this cross-talk/noise level tradeoff. Noise levels could be electronically filtered out at the expense of lowering the measurement frequency of the sensor, therefore the different BW optical filter coatings designs may be suited better to different applications with different measurement frequencies and accuracy requirements.

In addition to testing of improvement of gas sensor performance using multilayered optical coatings, coating uniformity and structural integrity tests under various environmental conditions were carried out. As mentioned, the multilayer filters were deposited onto full 4" Si wafers. The wafers were then diced and the optical transmittance of each section was measured, showing excellent thickness uniformities of +/-0.355% and +/-0.530% for 160 nm and 300 nm BW BP coatings respectively. This demonstrates that full production wafers can be successfully coated and subsequently diced without disruption to the optical coating, which suggests that full PD production wafers may also be coated prior to dicing. Witness samples (Si substrates) coated with

the multilayer thin film optical filter were then subjected to accelerated lifetime testing using a pressure cooker to expose the coating to high heat and high pressure for different lengths of time. The optical transmittance was measured after 5, 10, 20 and 40 minutes to observe the effect on the optical properties of the coating. It was found that no significant shift occurred up to 40 minutes, however a slight change in peak transmittance was observed, hypothesized to be due to absorption of H_2O into the film matrix. The witness samples were also subjected to less severe but longer duration temperature and humidity testing in an environmental chamber. The samples were subjected to a humidity test where they were exposed to 50°C and 95% RH for 24 hours, after which, the optical transmittance was measured. The temperature test comprised of exposing the coating to a temperature range of -40°C to 70°C where the temperature was held for 2 hours at each temperature and ramped up by 10°C every 2 hours – after this test the optical transmittance was also measured. For both the temperature and humidity tests, no significant change in the optical transmittance of the samples was observed suggesting that the deposited films are highly dense and are unlikely to undergo delamination in conditions in which the CH4 gas sensor would be present.

References

1. Mitchell, J.F.B. The "Greenhouse" effect and climate change. Rev. Geophys. 1989, 27, 115, doi:10.1029/RG027i001p00115.
2. Zhang, T.; Nix, M. B.; Yoo, B. Y.; Deshusses, M. A.; Myung, N. V. Electrochemically functionalized single-walled carbon nanotube gas sensor. Electroanalysis 2006, 18, 1153–1158, doi:10.1002/elan.200603527.
3. Christensen, T.H.; Cossu, R.; Stegmann, R. Chapter 3, Landfilling of waste: Biogas, 1st edition, Taylor & Francis, Oxford, England, 1996, 0419194002
4. Tchobanoglous, G; et al. Chapter 1, Integrated Solid Waste Management - Engineering Principles and Management Issues, 1st edition, King, P.H.; Eliassen, R. McGraw-Hill International editions, USA, 1993, 0071128654
5. Braker, W.; Mossman, A.L. Matheson Gas Data Book, 7th edition, Yaws, C.L, McGraw-Hill Professional, USA, 2001, **0071358544**
6. Britton, L.G. Using material data in static hazard assessment, Process Safety Progress, 1992, 1, 56-70, https://doi.org/10.1002/prsb.720110209
7. Dreisbach, F.; Staudt, R.; Keller, J. U. High pressure adsorption data of methane, nitrogen, carbon dioxide and their binary and ternary mixtures on activated carbon. Adsorption 1999, 5, 215–227, doi:10.1023/A:1008914703884.
8. Tadesse, K.; Smith, A.; Brydon, W. G.; Eastwood, M. Gas chormatographic technique for combined measurement of hydrogen and methane using thermal conductivity detector. J. Chromatogr. A 1979, 171, 416–418, doi:10.1016/S0021-9673(01)95325-7
9. Lee, J. H.; Trimm, D. L. Catalytic combustion of methane. Fuel Process. Technol. 1995, 42, 339–359, doi:10.1016/0378-3820(94)00091-7.
10. RAE Systems by Honeywell Staff The PID Handbook—Theory and Applications of Direct-Reading Photoionization Detectors (PIDs); 3rd ed.; 2013; ISBN 0976816210.
11. Zhu, Z.; Xu, Y.; Jiang, B. A one ppm NDIR methane gas sensor with single frequency filter denoising algorithm. Sensors (Switzerland) 2012, 12, 12729–12740, doi:10.3390/s120912729.
12. Tan, Q.; Tang, L.; Yang, M.; Xue, C.; Zhang, W.; Liu, J.; Xiong, J. Three-gas detection system

with IR optical sensor based on NDIR technology. Opt. Lasers Eng. 2015, 74, 103–108, doi:10.1016/j.optlaseng. 2015.05.007.

13. Hodgkinson, J.; Tatam, R. P. Optical gas sensing: A review. Meas. Sci. Technol. 2013, 24, 12004–59, doi:10.1088/0957-0233/24/1/012004.
14. Dinh, T. V.; Choi, I. Y.; Son, Y. S.; Kim, J. C. A review on non-dispersive infrared gas sensors: Improvement of sensor detection limit and interference correction. Sensors Actuators, B Chem. 2016, 231, 529–538, doi:10.1016/j.snb.2016.03.040.
15. Gas Sensing Solutions Available online: https://www.gassensing.co.uk/ (accessed on Jul 2, 2018).
16. A Novel Solid State Non-Dispersive Infrared CO_2 Gas Sensor Compatible with Wireless and Portable Deployment", D Gibson, C MacGregor, *Sensors*. 2013; 13(6):7079-7103 (May 2013).
17. Fleming, L.; Gibson, D.; Song, S.; Li, C.; Reid, S. Reducing N2O induced cross-talk in a NDIR CO2 gas sensor for breath analysis using multilayer thin film optical interference coatings. Surf. Coatings Technol. 2018, 336, 9–16, doi:10.1016/j.surfcoat.2017.09.033.
18. Gas Sensing Solutions. Available online: https://www.gassensing.co.uk / (accessed on 30/07/18)
19. Mipex Tech. Available online: https://mipex-tech.com (accessed on 30/07/18)
20. Rothman, L. S et al, J. The HITRAN 2008 molecular spectroscopic database. J. Quant. Spectrosc. Radiat. Transf. 2009, 110, 533–572, doi:10.1016/j.jqsrt.2009.02.013.
21. PTC Mathcad. Available online: https://www.ptc.com/en/products/mathcad (accessed on 30/07/18)
22. Smestad, G.P. Generalized model of a solar converter, Optoelectronics of Solar Cells, 1st edition, SPIE press, 2002
23. Smestad, G.; Ries, H. Luminescence and current-voltage characteristics of solar cells and optoelectronic devices. Sol. Energy Mater. Sol. Cells 1992, 25, 51–71, doi:10.1016/0927-0248(92)90016-I.
24. Rieke, G. Detection of Light; Cambridge University Press: Cambridge, 2002; ISBN 9780511606496.
25. O'Leary, S.K.; Johnson, S.R.; Lim, P.K. The relationship between the distribution of electronic states and the optical absorption spectrum of an amorphous semiconductor: An empirical analysis, J. Appl. Phys. 82, 3334 (1997); doi: 10.1063/1.365643
26. Li, C.; Song, S.; Gibson, D.; Child, D.; Chu, H. on; Waddell, E. Modeling and validation of uniform large-area optical coating deposition on a rotating drum using microwave plasma reactive sputtering. Appl. Opt. 2017, 56, C65, doi:10.1364/AO.56.000C65.
27. Pierre Bouguer, Essai d'optique sur la gradation de la lumière (Paris, France: Claude Jombert, 1729) pp. 16–22.
28. Fleming, L, 2018. Reducing N2O induced cross-talk in a NDIR CO2 gas sensor using multilayer thin film optical interference filters. Ph.D thesis. Paisley: The University of the West of Scotland
29. Software Spectra Inc. 2018. http://www.sspectra.com/. [ONLINE] Available at: http://www.sspectra.com/. [Accessed 20 September 2018].

30. Inficon. 2018. IC 5 thin film deposition controller manual. [ONLINE] Available at: https://products.inficon.com/getattachment.axd/?attaName=f23367c6-34f1-446a-814a-8327045d0c59. [Accessed 20 September 2018].